

UNCLASSIFIED

AD NUMBER

ADC003501

CLASSIFICATION CHANGES

TO: unclassified

FROM: secret

LIMITATION CHANGES

TO:
Approved for public release, distribution unlimited

FROM:
Distribution authorized to U.S. Gov't. agencies only; Foreign Government Information; 01 FEB 1974. Other requests shall be referred to Commander, Air Force Systems Command, Attn: SDE, Washington, DC 20334.

AUTHORITY

31 Dec 1984, per document marking; NRL Code/5309 memo dtd 20 Feb 1997

THIS PAGE IS UNCLASSIFIED



AD C 003501

SECRET

AN/FPS-95 RESEARCH AND DEVELOPMENT PROGRAM
(FINAL TECHNICAL REPORT, NAVAL RESEARCH
LABORATORY, NOISE/INTERFERENCE ENVIRONMENT) (U)

J. F. Thomason
Naval Research Laboratory
Washington, D. C. 20375

March 1974

DDC
RECEIVED
OCT 15 1975
RECEIVED
D C

Distribution limited to U.S. Gov't agencies only;
Foreign Information; 1 February 1974. Other requests
for this document must be referred to Hq AFSC (SDE).

NATIONAL SECURITY INFORMATION
Unauthorized Disclosure Subject to
Criminal Sanctions

506089
23

RECEIVED

SEP 4 1974

Classified by ESD/OC
Exempt from General Declassification
Schedule of Executive Order 11652 CA-3
Declassify on: 31 December 1984

NAVAL RESEARCH LABORATORY

Prepared for

DEPUTY FOR SURVEILLANCE AND CONTROL SYSTEMS
HQ ELECTRONIC SYSTEMS DIVISION (AFSC)
L. G. Hanscom Field, Bedford, MA 01730

DDC CONTROL
NO 52049

SECRET

DDC FILE COPY

ACCESSION for	
RTIS	White Section <input type="checkbox"/>
BBC	Buff Section <input checked="" type="checkbox"/>
UNANNOUNCED	<input type="checkbox"/>
JUSTIFIED	
SECRET	
BY	
DIS:	
Dist:	
B	

LEGAL NOTICE

When U.S. Government drawings, specifications or other data are used for any purpose other than a definitely related government procurement operation, the government thereby incurs no responsibility nor any obligation whatsoever; and the fact that the government may have formulated, furnished, or in any way supplied the said drawings, specifications, or other data is not to be regarded by implication or otherwise as in any manner licensing the holder or any other person or conveying any rights or permission to manufacture, use, or sell any patented invention that may in any way be related thereto.

OTHER NOTICES

Do not return this copy. Retain or destroy, in accordance with pertinent Security Regulations.

This technical report has been reviewed and is approved for publication.

JM Headrick
 JAMES M. HEADRICK, Branch Head
 Radar Techniques Branch
 Radar Division, Naval Research Laboratory

Richard W. Coraine
 RICHARD W. CORAINE, Lt Col, USAF
 Chief, 441 A
 Engineering Division

FOR THE COMMANDER
Donald W. Lambrecht
 DONALD W. LAMBRECHT, Colonel, USAF
 System Program Director

SECRET

SECRET

18 ESD

19 TR-73-270-Vol-2-Pl-E

2

SECURITY CLASSIFICATION OF THIS PAGE (When Data Entered)

REPORT DOCUMENTATION PAGE		READ INSTRUCTIONS BEFORE COMPLETING FORM
1. REPORT NUMBER NRL Memorandum Report 2715	2. GOVT ACCESSION NO.	3. RECIPIENT'S CATALOG NUMBER 9 Rept. for 1971-1973
4. TITLE (and Subtitle) AN/FPS-95 RESEARCH AND DEVELOPMENT PROGRAM (FINAL TECHNICAL REPORT, NAVAL RESEARCH LABORATORY, NOISE/ INTERFERENCE ENVIRONMENT) (U) - 8		5. TYPE OF REPORT & PERIOD COVERED Final report covering period 1971-1973
7. AUTHOR(s) 10 Joe F. Thomason		6. PERFORMING ORG. REPORT NUMBER
9. PERFORMING ORGANIZATION NAME AND ADDRESS Naval Research Laboratory Washington, D. C. 20375		8. CONTRACT OR GRANT NUMBER(s) USAF DODR 227507300001
11. CONTROLLING OFFICE NAME AND ADDRESS Deputy for Surveillance and Control Systems Hq Electronic Systems Division, L. G. Hall Fld, MA		10. PROGRAM ELEMENT, PROJECT, TASK AREA & WORK UNIT NUMBERS 16 NRL- XXXXXX PR02-42
14. MONITORING AGENCY NAME & ADDRESS (if different from Controlling Office) Hq AFSC (SDE) Andrews AFB, Washington, D. C. 20334		12. REPORT DATE March 1974
		13. NUMBER OF PAGES 34
		15. SECURITY CLASS. (of this report) SECRET
16. DISTRIBUTION STATEMENT (of this Report) Distribution limited to U.S. Gov't agencies only; Foreign Information; 1 February 1974. Other requests for this document must be referred to Hq AFSC (SDE).		15a. DECLASSIFICATION/DOWNGRADING SCHEDULE Exempt-Exemp Cat: 3
17. DISTRIBUTION STATEMENT (of the abstract entered in Block 20, if different from Report)		D D C RECEIVED OCT 15 1975 D
18. SUPPLEMENTARY NOTES		
19. KEY WORDS (Continue on reverse side if necessary and identify by block number) Over-the-horizon radar Radar noise Meteor reflections		
20. ABSTRACT (Continue on reverse side if necessary and identify by block number) (SECRET) The operational performance of the AN/FPS-95 was degraded by the appearance of an enhanced noise which occurred in conjunction with the back-scatter. The present paper describes the experimental attempt to identify that component of the noise which could arise from near range phenomena. For 23 MHz, the cause is due primarily to line-of-sight meteor trail reflections, while for lower operating frequencies there are indications of spreading of surface wave clutter by antenna vibration.		

DD FORM 1 JAN 73 1473

EDITION OF 1 NOV 65 IS OBSOLETE
S/N 0102-014-6601

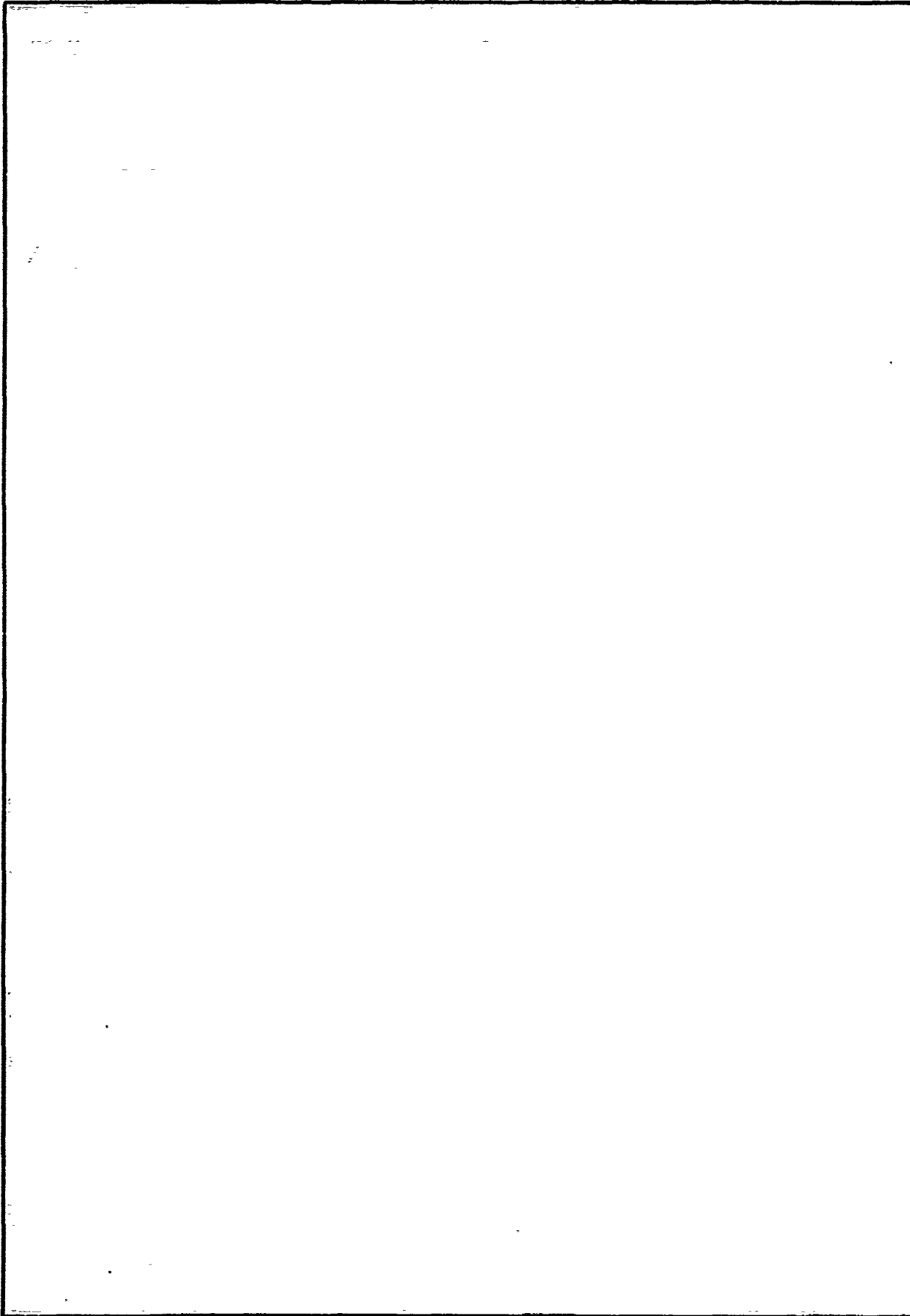
SECRET

SECURITY CLASSIFICATION OF THIS PAGE (When Data Entered)

257950

SECRET

SECURITY CLASSIFICATION OF THIS PAGE(When Data Entered)



SECRET

SECURITY CLASSIFICATION OF THIS PAGE(When Data Entered)

SECRET

TABLE OF CONTENTS

	<u>Page</u>
Abstract	iv
I. INTRODUCTION	1
II. TRANSMIT/RECEIVE SWITCH DEIONIZATION	1
III. TRANSMITTER-INDUCED CORONA	1
IV. ANTENNA VIBRATION	2
V. METEORS	2
A. Identification of Near-Range Noise Sources	3
B. Spectral Characteristics of Meteor Returns	4
C. A Multiplicative Noise Burst	5
D. Antenna Elevation Patterns Derived from Meteor Data	5
E. Determination of Scattering Coefficient for the Meteor Flux	7
VI. CONCLUSIONS	8
VII. RECOMMENDATIONS FOR FUTURE WORK	9
VIII. ACKNOWLEDGMENTS	9

SECRET

ABSTRACT
(Secret)

The operational performance of the AN/FPS-95 was degraded by the appearance of an enhanced noise which occurred in conjunction with the backscatter. The present paper describes the experimental attempt to identify that component of the noise which could arise from near range phenomena. For 23 MHz, the cause is due primarily to line-of-sight meteor trail reflections, while for lower operating frequencies there are indications of spreading of surface wave clutter by antenna vibration.

* * *

This report represents work performed by the Naval Research Laboratory (NRL) to carry out for the U. S. Air Force the investigation of certain Over-the-Horizon (OTH) techniques using the AN/FPS-95 Radar. This Research and Development (R&D) work was conducted by NRL in direct technical support to the Over-the-Horizon Program Office (OCS) of the Electronic Systems Division (AFSC).

SECRET

FINAL TECHNICAL REPORT ON THE AN/FPS-95 RESEARCH AND DEVELOPMENT PROGRAM
Vol. II, Part E. NOISE/INTERFERENCE ENVIRONMENT (U)

I. INTRODUCTION (U)

(S) During the course of its first year's operation the performance of the AN/FPS-95 was degraded by the occurrence of an enhanced noise which appeared in conjunction with the backscatter. To determine the causes of this "clutter-related noise" the ESD Scientific Assessment Committee was established in January 1973. A test plan was developed consisting of seven specific experiments. The present paper is a report on the experiment to identify the source of that component of the excess noise that could occur in the near range.

(S) The mechanisms postulated by the Scientific Assessment Committee for the production of the short-range noise were transmit/receive switch deionization, transmitter-induced corona, antenna vibration, and meteors. That portion of the noise appearing in the skip zone just short of the clutter is thought to be clutter related and is excluded from consideration for this test.

II. TRANSMIT/RECEIVE SWITCH DEIONIZATION (U)

(S) Extensive tests were performed on the receiver and the transmit/receive switch during the Category II tests and DVST. These tests show that the solid state duplexer has no measurable effect after 24 microseconds from its turnoff time. However, these tests also show a set of transients associated with gating the receiver off during the transmit pulse period. This gate has a rise time on the order of 100 nanoseconds and gates any signal present in the receiver preselector passband. Sidebands generated by gating signals in the preselector passband appear in the receiver passband. Because the time constant associated with these sidebands is that of the crystal filter in the receiver, only the first and last range samples are contaminated. However, the postdetection filter in the on-line signal processor has a much longer time constant and smears the transient over several range cells if the transient is allowed to reach the processor. During the DVST period the receiver gating was modified to limit receiver off-time to the transmission interval. Gating of data to the signal processor was provided by restricting the range samples sent to the digital-to-analog converter. This modification alleviated the on-line near-range noise problem somewhat. As will be seen from data presented later in this report, for off-line signal processing, where range samples are treated independently, the transient contaminates only the first range cell.

III. TRANSMITTER-INDUCED CORONA (U)

(S) Corona detection tests were run on 13 March 1973 between 0800Z and 0930Z. The detection equipment used was a Singer NM-25T, radio interference field intensity measuring equipment. The NM-25T was mounted on the platform outside of door 8. Door 8 is in the antenna backlobe in line with string 4. While operating the radar at full power the NM-25T was used to scan the frequency range from 150 kHz to 30 MHz for signals produced by antenna corona.

SECRET

Although the low frequency part of the spectrum was thought to be the most sensitive indicator of the presence of antenna corona, no signals related to the AN/FPS-95 operation could be found in this part of the spectrum. However, with the system operating on 6.97 MHz evidence of antenna corona was found by listening to the fourth harmonic at 27.9 MHz. The level of this harmonic was greatly influenced by the power level of transmitter operation and by the particular antenna string in use. This is apparently the antenna corona or arcing which produces harmonics up into the television broadcast band and has caused television interference in the vicinity when operating below 10.5 MHz. This corona has been the subject of an internal investigation as the result of its link with the television interference. Numerous photographs and measurements have been made by the investigators. Although the television interference investigation had established a cutoff frequency of about 10.5 MHz for the effect of antenna arcing on television reception, attempts were made to detect evidence of corona when operating above 10.5 MHz. When operating on 15 MHz and scanning from 150 kHz to the second harmonic, no evidence of antenna corona could be found. Therefore, testing at 23 MHz for the antenna vibration and meteor hypothesis continued without the installation of a corona monitor. There appears to be nothing to monitor.

IV. ANTENNA VIBRATION (U)

(S) Several attempts were made to obtain a sufficient surface-wave-clutter-to-background-noise ratio to see clutter-related noise. Typically, 30 or 40 dB clutter-to-noise ratio was achieved by operating at a low frequency on vertical polarization. For example, on 7.71 MHz with a 250- μ s pulse the surface wave clutter was -40 dBm at 80 nmi. Background noise for this data at 40 PRF and 10 seconds integration time was about -74 dBm. Data taken in this frequency range show an interesting fluctuation in the noise which appears to be associated with the surface wave clutter. The tests are inconclusive because of the possible contamination of the first range cell by gating transient already discussed.

(S) Figure 2 which is described in detail later shows data taken at 23 MHz on 80 PRF which contains a -69 dBm surface wave clutter signal at 40 nmi. Although the background noise for this data was down to about -130 dBm, there was no evidence of spectral spreading of the surface wave clutter. No surface wave clutter was observable on the system antenna when operating the antenna horizontally polarized or when operating on the Yagi.

V. METEORS (U)

(U) Meteoric particles impinging on the atmosphere produce ionization trails at 80- to 110-km altitude which result in radar echoes in the near range. Because of the large numbers of these echoes and their spread spectrum nature, they are noise-like in character. The earth intercepts approximately 10^{12} meteoric particles per day ranging in mass from 10^{-8} to 10^4 grams which produce electron line densities above 10^{10} electrons per meter. The

SECRET

product of the number of meteors of a given mass or greater and that mass has been found to be roughly constant at 10^5 grams. Since the electron line density produced by a specific meteoric particle is directly proportional to that particle's mass, a similar relationship holds between the meteor rate and the electron density. Equation 1 gives the relationship between N_e , the number of meteors per day producing a line electron density of D_e electrons per meter or greater and the electron density D_e

$$D_e N_e = 10^{22} \quad (1)$$

(U) Meteoric particles produce electron densities from about 10^{10} electrons per meter upwards. Assuming the system can detect meteor trails from this density upwards, the rate of occurrence R_e may be calculated

$$R_e = \frac{10^{22} A_r}{D_e A_e} \quad (2)$$

where A_r is the area in one resolution cell and A_e is the area of the earth. Evaluating the equation in dB for an electron density of 10^{10} electrons per meter, $D_e = 100$ dB, $A_e = 147$ dBsm, and $A_r = 93$ dBsm. This resolution cell represents one 20-nmi range cell at 280 nmi with an antenna beamwidth of 6° . The resulting rate R_e is 66 dB or $10^{6.6}$ meteors per day. This may be reduced to a more meaningful rate of $10^{1.6}$ meteors per second for a typical resolution cell. Since the radar reflections are produced in a rather narrow altitude band, the elevation angle antenna pattern is reflected in the amplitude-range distribution of radar returns from this meteor flux.

A. Identification of Near-Range Noise Sources (U)

(S) To test the meteor hypothesis a series of tests were performed in which the operating frequency was held constant at about 23 MHz and, by varying the time of day, data were taken both above and below the maximum usable frequency. Figure 1 shows one set of data taken above the ground backscatter MUF using the Stanford Research Institute Facsimile processor. Data are displayed in the form of range-time-intensity plots. The MDS for this setup is -115 dBm. The reduction in the range at which the near-range noise appears when switching from vertical to horizontal antenna polarization is apparent and is consistent with the meteor hypothesis. This shift in range is the result of the higher elevation pattern of the horizontally polarized system antenna as compared to the vertically polarized system antenna. The transmitters were turned off between each run to confirm that the noise being seen was in fact a radar return. In a paper which appeared in the IRE Proceedings in October of 1955, O. G. Villard et al published plots of the expected and observed meteor activity as a function of azimuth from a radar at Stanford University. These plots were for a radar located at 37.5° north latitude in the month of June and show a higher intensity of meteors toward the north. Figure 1 also shows a similar higher density in Beam 1 which is the more northerly beam. A close examination of Figure 1

SECRET

shows a -100 dBm track beginning at about 0606Z and continuing until 0610Z when the transmitters were shut down. The radar range is about 100 nmi. Observation of the on-line system doppler-versus-range displays during this period showed a strong line-of-sight aircraft target at 100 nmi. Thus, this and other weaker tracks are attributed to line-of-sight aircraft. These weaker tracks are removed for the purpose of the meteor analysis by the use of median signal analysis. This analysis is described in later sections.

(S) In addition to the general shortening of the range to the maximum noise density a close examination of the data for beam 1 - vertical shows a null at 275 nmi. If a meteor belt altitude of 95 km is assumed this range corresponds to an elevation angle of 8.5° . Measurements made by Mr. Carmen Malagisi in August 1971 indicate a null in beam 1 - vertical elevation antenna pattern at 9.5° . Because of difficulties in integrating over a long period of time with the facsimile display and taking measurements of signal levels off of it, a more detailed analysis requires a different signal processing and display scheme. This analysis is described in the next section.

B. Spectral Characteristics of Meteor Returns (U)

(S) Figures 2, 3 and 4 are plots of doppler-range-power, with power in each doppler-range cell being shown by a single character. A blank indicates that the power in that particular doppler-range cell was below the -135 dBm threshold chosen for these plots. The number zero indicates a power above the threshold but not more than 3 dB above. The other numbers and the letters are used similarly in steps of 3 dB. Doppler frequency is shown along the bottom of the plot with zero at each edge. The entire doppler extent is being displayed. Range runs from 40 nmi in steps of 20 nmi. These figures are composites, each composed of 120 separate 3.2-second integration times combined by averaging power over time in the frequency domain. Since the pulse length for this data was 250 μ s, no sample averaging was used. During the period when the data for these figures were taken the operating frequency was 23 MHz which was above the maximum usable frequency.

(S) Operation above the maximum usable frequency allowed use of a pulse repetition frequency of 80 Hz without the possibility of contamination of the near-range noise data from long-range clutter and noise sources being time folded into the near range. This PRF allows a higher maximum unambiguous doppler frequency than is practical to use below the MUF, thus more accurately characterizing the frequency components in the returns. The actual PRF used for this series of figures, 80 Hz, gives a maximum unambiguous doppler of ± 40 Hz. An examination of the figures shows that most of the energy from the meteor activity is concentrated within ± 20 Hz of zero frequency. These figures also confirm the shift in amplitude versus range characteristic when antenna elevation patterns are changed. In a later section, it is shown that the echoes in these illustrations approximately match those expected based on the assumed meteor flux and antenna patterns. Deviations are attributed to imperfections in the antenna patterns.

SECRET

C. A Multiplicative Noise Burst (U)

(S) In order to take data below the maximum usable frequency a very low pulse repetition frequency is required to unfold all of the clutter and noise sources thus insuring that the near-range noise data are not contaminated by time-folded returns. The data shown in Figures 5, 6 and 7 were taken with a pulse repetition frequency of 10 Hz which gives a maximum unambiguous range of 8000 nmi. The format for these figures is similar to that used in Figures 2, 3 and 4 except for the very restricted doppler extent. Again each figure represents a 6.4-minute average. In this case the incoherent average is composed of 30 separate integration periods of 12.8 seconds each. In each of the figures ground backscatter is visible from about 1200 nmi to 1900 nmi. The near-range noise amplitude-range distribution undergoes the same shifts in range as seen in previous figures. However, Figure 5 shows a large amount of noise in the range 1300 to 1800 nmi which seems to be multiplicative because its amplitude-range appears to correlate well with clutter amplitude-range. To investigate the source of this noise the 30 integration periods which made up the 6.4-minute average were examined individually. Figure 8 shows the single integration time found to contain the multiplicative noise. Since the interruption of one transmit module could cause a noise burst similar to this one, the indicators of transmitter status written into the header on the raw data tape were examined. They showed no evidence of transmitter interruption. Figure 9 shows a two-minute average on beam 13V and is included to indicate the appearance of long-term averages on beam 13, vertical which do not include the multiplicative noise bursts. Although this noise phenomenon may not be typical, it was included because it may represent one of the sources of far-range noise contamination. Since this did not represent a near-range phenomenon, it was not investigated further.

D. Antenna Elevation Patterns Derived from Meteor Data (U)

(U) In order to gain something more useful than the mere identification of the near-range noise, which is considered to have been accomplished by showing the gross shift in range as antenna elevation pattern is changed, the meteor data taken at 10 PRF and shown in Figures 5, 6 and 7 have been reduced to provide elevation antenna patterns of beam 13, both vertical and horizontal polarization, and of the Yagi. From this data and assuming that the Yagi produces its theoretical lobe-maximum gain and that the near-range noise is predominantly meteors, a scattering coefficient σ_m^0 for the meteor flux has been calculated.

(S) Figure 10 shows the same data as was previously shown in Figure 5 except that the signal level in each range cell has been reduced to a single number. This was accomplished by separating the 10-Hz doppler extent available into 4 segments each 2.5 Hz wide. For each of 30 integration times a median signal level was determined for each segment. These four medians were then averaged over the thirty integration periods to produce a 6.4-minute average.

SECRET

Because the energy from the meteor returns has been seen to be rather well spread over the 10-Hz doppler extent, the median is a good measure of signal strength while eliminating CW and aircraft targets which would contaminate a total power measure. The DC offset which appears at some frequency is eliminated by not including that segment covering zero frequency when finally combining the remaining three medians to produce a single measure of the signal in each range cell.

(U) Before the signal levels shown in Figure 10 can be used to plot the antenna elevation pattern, they must be normalized to remove the range-spreading factor. Figure 11 shows the factor used to normalize the received signals to that expected from a distributed target at 200 nmi. Figure 12 shows the relationship between slant range and elevation angle used to establish the elevation angle. Figure 13 is the result of applying these two figures to Figure 10 and plotting the signal levels relative to the maximum return which occurred at 280 nmi. The dB scale shown is half that used to plot the data points thus showing one-way antenna gain. Antenna elevation patterns determined in this way assume the scattering coefficient for the meteor flux to be constant as a function of elevation angle. For the angles between 4° and 25° which were used here this assumption probably does not distort the skirts of the patterns very much. For this set of data, the angle extent over which the data are valid is from about 4° to about 25° . The high angle limit results from the switching transient which contaminates the first range sample. The low angle limit results from an accumulation of spreading loss, which reduces signals to levels comparable to the noise in the skip zone produced by other users.

(U) Figure 14 presents a measured elevation pattern for beam 12, vertical. The elevation pattern for beam 13 was not measured. This figure shows a peak at 9.5° which compares rather well with the peak derived from the meteor data and shown in Figure 13.

(U) Figures 15 and 16 show the raw median data and the derived elevation pattern for beam 13, horizontal. Figure 17 shows the measured elevation pattern for beam 7. Again the beam 13, horizontal, pattern was not measured. The elevation pattern for beam 7, horizontal, is taken to be representative of the antenna when operating horizontally polarized. A comparison of the measured pattern with the one derived from the meteor data indicates a rather good agreement in the position of the pattern nulls and an interesting deformation of the shape of the main lobe. Whether the deformation is real or is an artifact introduced by this particular meteor data is unknown. Since the antenna gain in Figure 16 is plotted relative to the maximum gain of beam 13, vertical, it is apparent from Figure 16 that the absolute gain of beam 13 is reduced by about 1 dB when using horizontal polarization.

(S) Figures 18 and 19 show the raw median data and the derived elevation pattern for the Yagi. Measured azimuth patterns indicate that the beamwidth for beam 13 at 23 MHz is about 6° . The half-power beamwidth for the Yagi has been measured to be about 36° . If a single meteor trail were

SECRET

being examined, its radar cross section would not depend on antenna beamwidth. However, since the averaged data represent the effects of on the order of 10^4 meteors per range cell, the meteor flux must be considered an area phenomenon. Solving the radar equation for the antenna gain G

$$G = \left(\frac{(4\pi)^3 R^4 P_R}{\lambda^2 P_T \sigma} \right)^{1/2} \quad (3)$$

In this equation R is the range to the target, P_R is the received power, λ is the wavelength, P_T is the transmitted power, and σ is the target radar cross section. For distributed targets the radar cross section σ is considered in terms of the target area and a scattering coefficient representing the radar cross section of a unit area. Thus

$$\sigma = \sigma^0 R B_w \Delta R \quad (4)$$

where σ^0 is the scattering coefficient and the area for this particular situation is the resolution cell size. The resolution cell is formed by the antenna half-power beamwidth B_w (radians), the range to the target R, and the range resolution ΔR . Substituting equation (4) into equation (3)

$$G = \left(\frac{(4\pi)^3 R^3 P_R}{\lambda^2 P_T \sigma^0 B_w \Delta R} \right)^{1/2} \quad (5)$$

(S) From equation (5) it may be seen that although Yagi operation has a factor of 6 decrease in transmit power, because the Yagi uses only one of the six transmitter modules, this decrease is offset by a factor of 6 increase in antenna half-power beamwidth. Having made the corrections necessary to allow an absolute gain comparison between the Yagi and the system antenna, note from Figure 19 that the maximum gain of the Yagi is about 4 dB below the maximum gain for beam 13, vertical. If the theoretical gain of the Yagi of 19 dBi is realized, the system antenna gain is 23 dBi for 23 MHz. Gain for beam 13, horizontal works out to about 1 dB lower at 22 dBi.

(U) Figure 20 shows the Yagi elevation pattern courtesy R. Rafuse. Comparison of Figure 19, the elevation pattern derived from meteor data, with Figure 20 reveals that the elevation patterns shown in the two figures agree fairly well.

E. Determination of Scattering Coefficient for the Meteor Flux (U)

(U) Equation (4) made use of a term σ^0 which represented the radar cross section per unit area for a distributed target. For earth backscatter this factor, σ^0 , is about -17 dB. The meteor data taken as part of this test

SECRET

allows the calculation of a similar factor σ_m^0 for the meteor flux. Figure 10 gives -120 dBm as the median signal level at the range where meteor activity is strongest, 280 nmi. The meteor flux produces a radar return that is spread rather uniformly over the entire 10-Hz doppler extent. The signal processing used for this data divided the spectrum into 128 doppler cells. Therefore, the equivalent coherent received signal is -120 + 21 or -99 dBm. Solving equation (5) for σ^0 the scattering coefficient

$$\sigma^0 = \frac{(4\pi)^3 R^3 P_R}{G^2 \lambda^2 B_w \Delta R P_T} \quad (6)$$

where R is the range to the target, P_R is the received power, G is the antenna gain, λ is the wavelength, B_w is the half-power beamwidth (in radians), ΔR is the range resolution and P_T is the transmit power. Evaluating the equation in dB gives $P_T = 96$ dBm, $P_R = -99$ dBm, $G^2 = 46$ dBi, $\lambda^2 = 22.3$ dBsm, $(4\pi)^3 = 33$ dB, $R^3 = 171$ dB, $B_w = -9.8$ dB, and $\Delta R = 45.7$ dB. The scattering coefficient σ_m^0 is then -94.8 dB. The data from which this coefficient was derived were taken during mid-March at about 0700 local time in beam 13.

(U) Certain cautions should be observed in using the meteor scattering coefficient. Because the meteor is a diffuse or spread signal rather than a coherent return, the appropriate adjustments must be made for the signal processing used. Thus if the spectrum extent occupied by the meteor returns is divided into 128 doppler cells, the signal level calculated from σ_m^0 must be reduced by 21 dB. Diurnal and azimuthal variations of σ_m^0 are expected.

VI. CONCLUSIONS (U)

(S) Certainly sufficient evidence has been gathered to confirm that for 23 MHz the near-range noise results primarily from line-of-sight meteor trail reflections. To a lesser extent line-of-sight aircraft and a switching transient contribute to the "noise" in the very near range.

(S) For the lower operating frequencies, there are indications of the possibility of spreading of surface wave clutter by antenna vibration. Further testing is required to determine whether this is indeed the case. No spreading of surface wave clutter above a clutter-to-noise ratio of 66 dB was observed at 23 MHz.

(S) Antenna corona does not appear to be a factor above 10.5 MHz. Corona existing below 10.5 MHz, because of its connection with television interference, is the subject of an intensive continuing investigation which will be reported separately.

(S) The absolute antenna gain for beam 13, vertical was estimated to be 23 dBi. Various elevation patterns measured by Mr. Carmen Malagisi in the summer of 1971 were confirmed. A scattering cross section, σ_m^0 for the meteor flux was determined to be -94.8 dB.

SECRET

VII. RECOMMENDATIONS FOR FUTURE WORK (U)

(U) Much valuable information would be gained from a program to measure the elevation pattern as a function of frequency for each of the beams that compose the system antenna. By making use of the meteor flux this may be accomplished with about 10 minutes of system time for each pattern desired. An analysis of the variations in the elevation patterns between beams and on different frequencies would be valuable in assessing the proper functioning of the antenna itself.

(S) The propagation prediction program and the raytracing programs currently use an idealized elevation pattern based on the assumption that the antenna system design goal of a frequency and beam-independent elevation pattern had been met. Analysis of Mr. Malagisi's measured elevation patterns supported by the patterns derived from meteor data indicates that this is a very bad assumption. Both the propagation prediction program and the raytracing programs should be fitted with a more realistic model of the antenna elevation patterns.

(U) The indications of noise introduced by antenna vibration when using the lower operating frequencies should certainly be pursued by further testing.

VIII. ACKNOWLEDGMENTS (U)

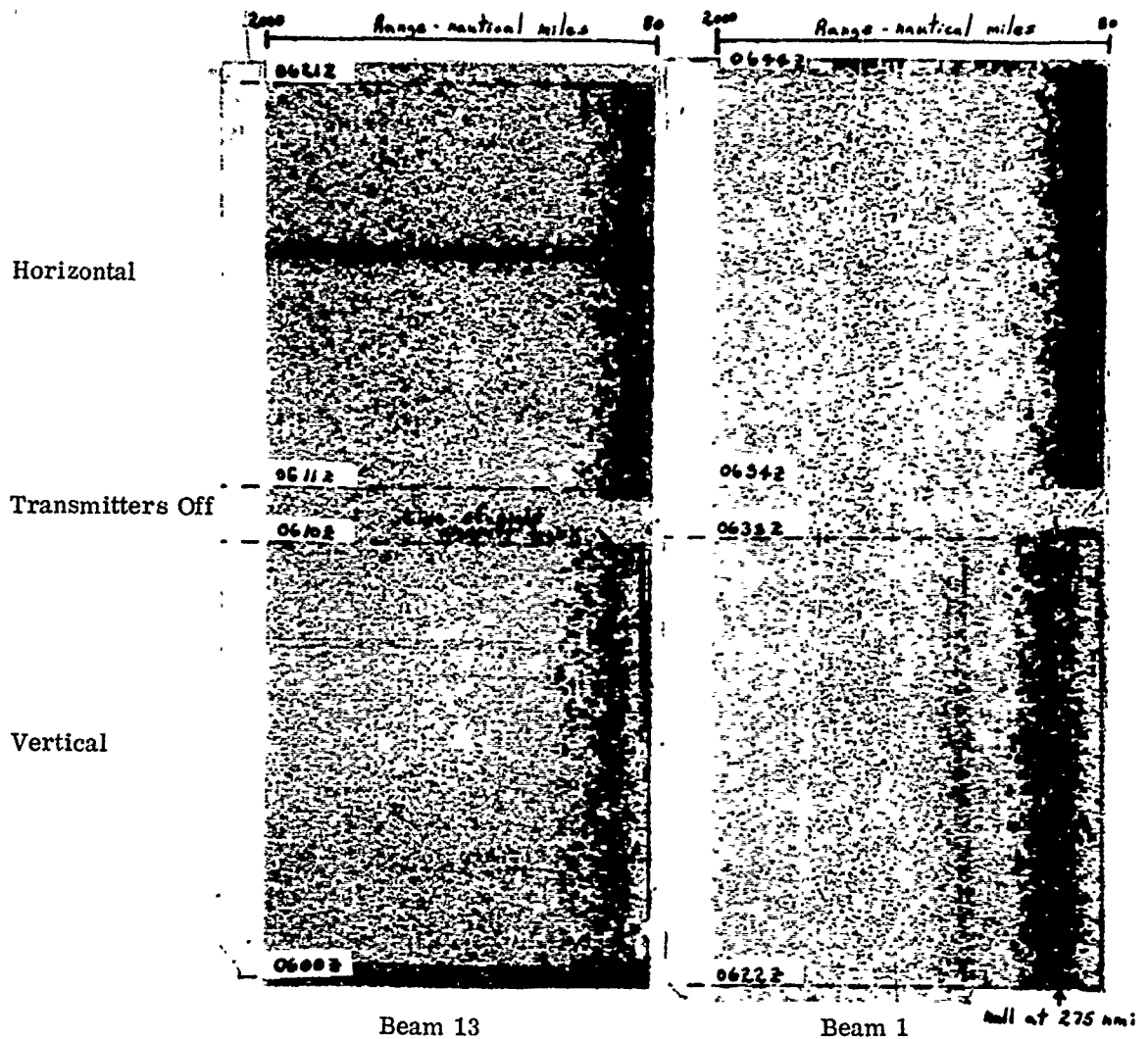
(U) The author would like to acknowledge the assistance of CAPT Mike Podhajecki who assisted in the data acquisition phase of the test. The signal processing routines used were written by Mr. James Hudnall with special modifications for signal averaging by CAPT Mark Clausen. The statistics routines used to determine median signal levels were supplied by Mr. Paul Shannon.

SECRET

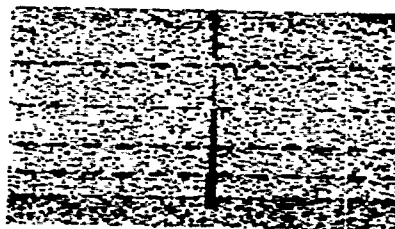
REFERENCES

1. Joseph Parr, "Antenna Patterns, Project COBRA MIST," Volumes 1 and 2, Rome Air Development Center, July 1972, UNCLASSIFIED.
2. C. T. Horne and G. H. Millman, "The Characteristics of Overdense Meteors at HF Backscatter Radar," Proceedings of the OHD Technical Review Meeting of 17-18 March 1971, Vol. I, SECRET.
3. O. G. Villard, et al, "The Role of Meteors in Extended Range VHF Propagation," Proceedings of the IRE, October 1955, UNCLASSIFIED.

SECRET



Operating frequency 23 MHz
250 μ s pulse

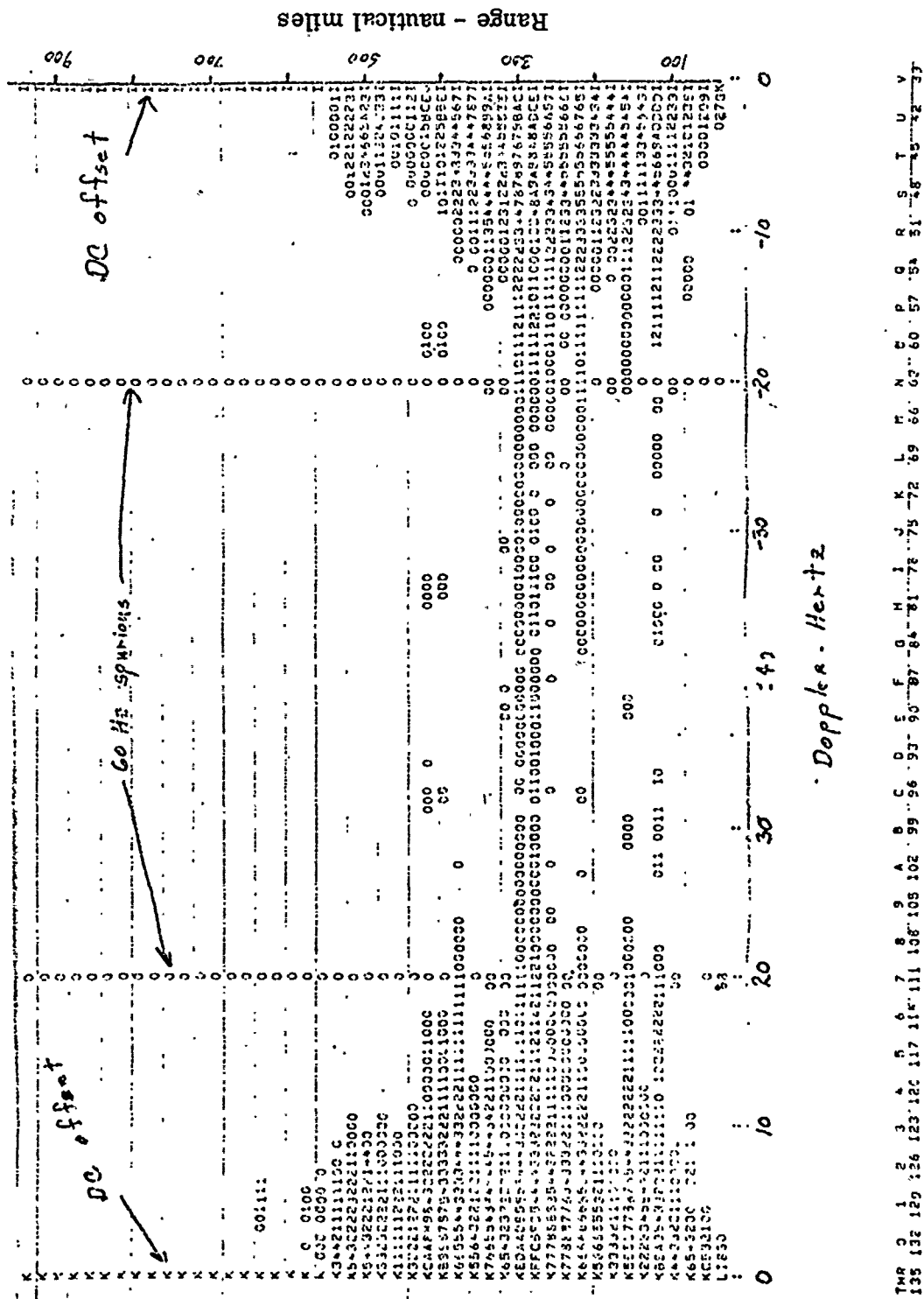


Simulated target level
-115 dBm
-120 dBm
-110 dBm
-100 dBm
-90 dBm

(C) Fig. 1 - SRI-Fax output

Copy available to DDC does not permit fully legible reproduction

SECRET

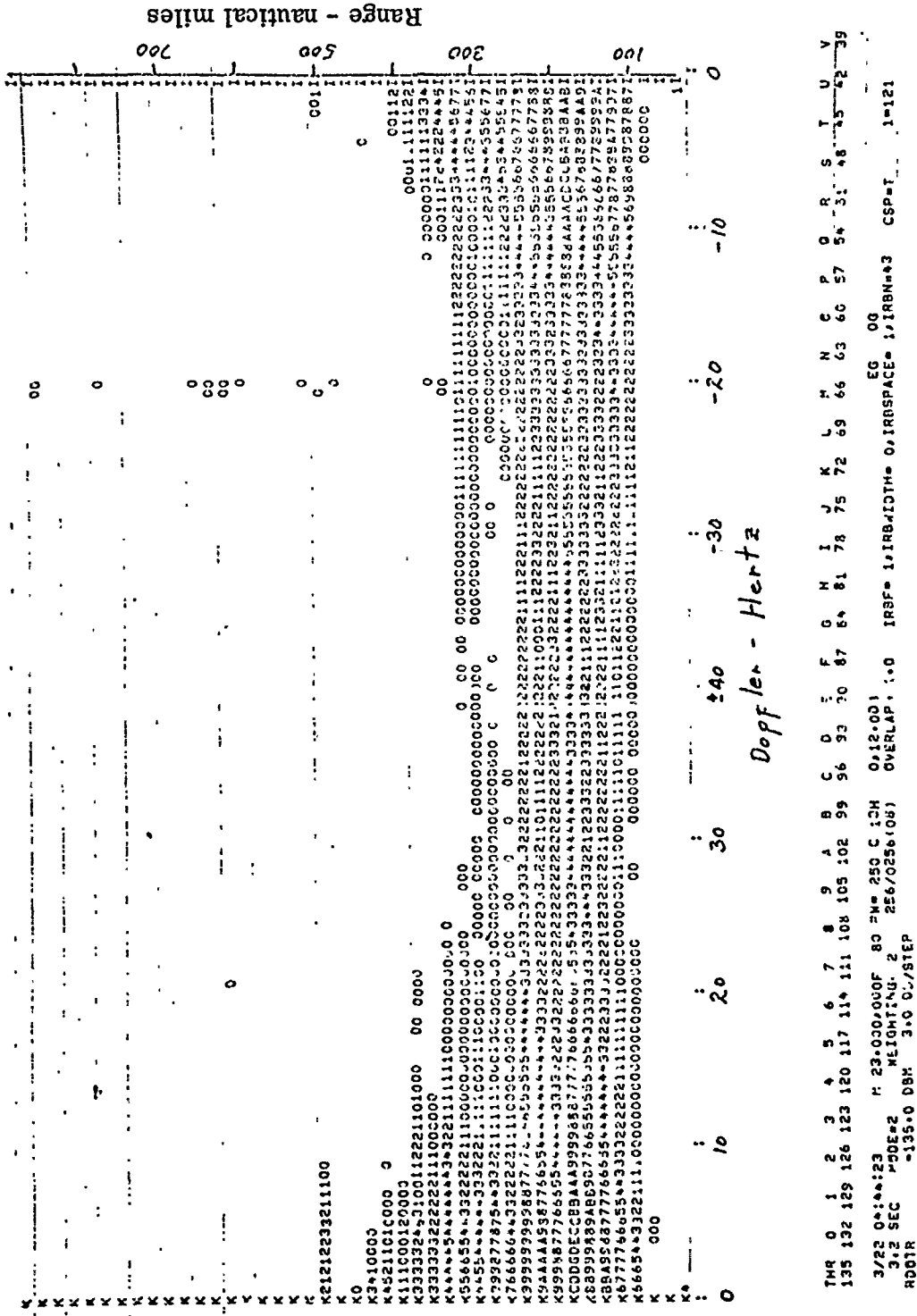


TMR 0 1 2 3 4 5 6 7 8 9 A B C D E F G H I J K L M N O P Q R S T U V
 135 132 129 126 123 120 117 114 111 108 105 102 99 96 93 90 87 84 81 78 75 72 69 66 63 60 57 54 51 48 45 42 39

3/22 C=12:53 M 23+000/000F 80 PWR 250 C 13V 0.12+029 EG CG
 3+2 SEC MODE=2 WLFU=11.03 2 556/255A1291 OVERLAP= 1-0 IPRF= 1:1:REWIDTH= 0.1:SSPACES= 1:IPRQ=66 CSP=1 1-121
 RCD14 -133.0 CW J=0 CR/STEP

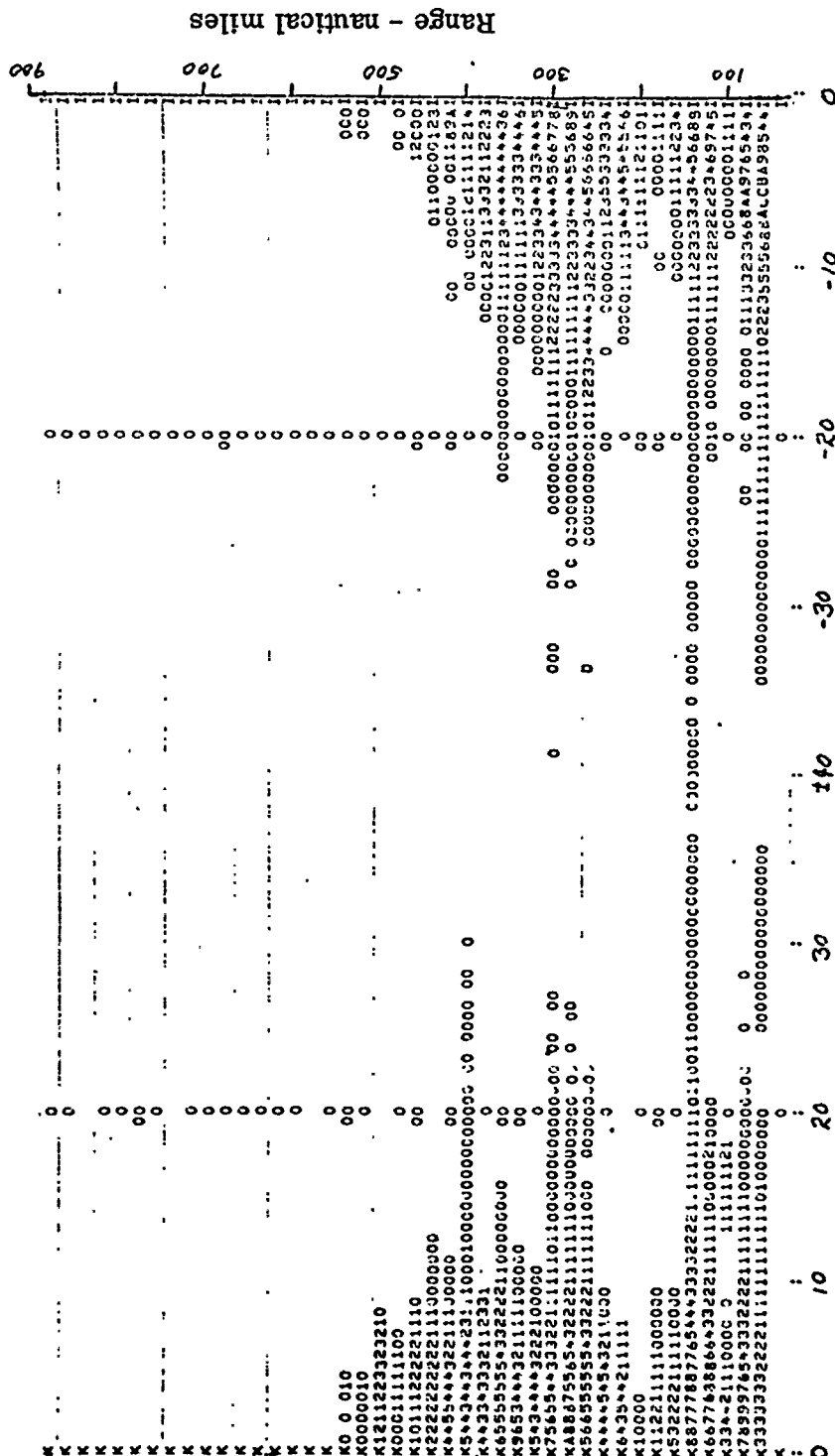
Threshold = -135 dBm Beam 13 Vertical
 Scale = 3 dB per step 6.4 minute average
 (U) Fig. 2 - Beam 13, Vertical, 80 PRF, 6.4-minute average.

SECRET



SECRET

SECRET



THR 0 1 2 3 4 5 6 7 8 9 A B C D E F G H I J K L M N O P Q R S T U V
 135 132 129 126 123 120 117 114 111 108 105 102 99 96 93 90 87 84 81 78 75 72 69 66 63 60 57 54 51 48 45 42 39

3/22 05:00:32 P 23.000/00F 80 FMS 250 C 13Y 0.12.CDF
 3.2 SEC HDE#2 WEIGHTING# 2 256/0256(08) OVERLAP. 1.0 :RRF# :IPB#IDTH# 0.1RSPACE= 1.1RBN##3 CSP#7 1-121
 ROOTH -135.0 DBM 3.0 CB/STEP

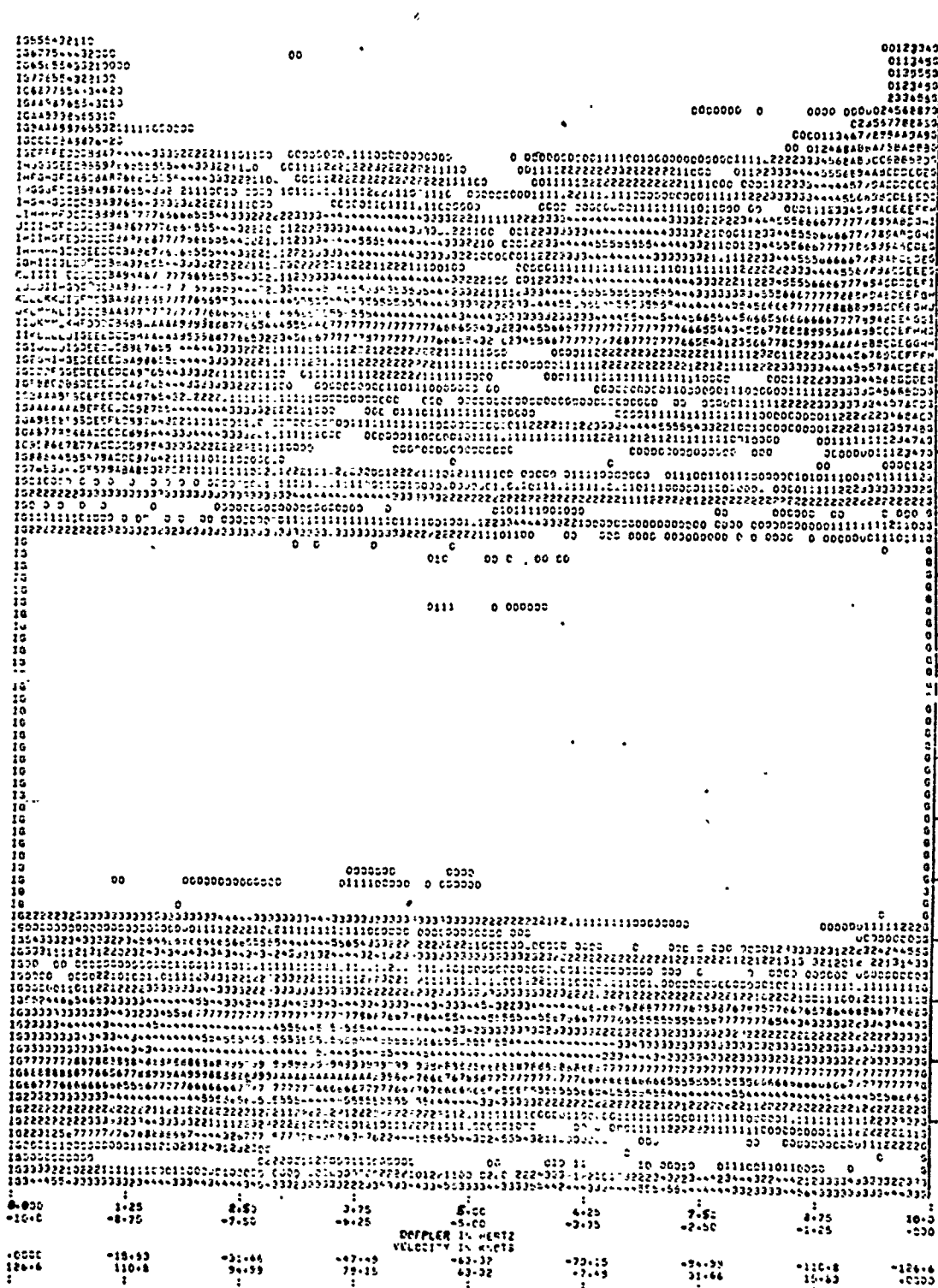
Threshold = -135 dBm
 Scale = 3 dB per step
 Yagi
 6.4 minute average
 (U) Fig. 4 - Yagi, 80 PRF, 6.4-minute average.

SECRET

Copy available to DDC does not permit fully legible reproduction

SECRET

1 2 3 4 5 6 7 8 9 A B C D E F G H I J K L M N O P Q R S T U V
10 11 12 13 14 15 16 17 18 19 20 21 22 23 24 25 26 27 28 29 30 31 32 33 34 35 36 37 38 39 40
374 17120129 M 23.000000 IC Fwv 250 C 13V 0.12-CDB EG CC
12.4 SEC -3.5E-2 -1.15MINS-2 128/01281071 OVERLAP- 1.0 REF= 171K51077-0.1785PACC- 17128439 CSP-T 1-031
00274 -128.0 Do 3.0 DB/STEP



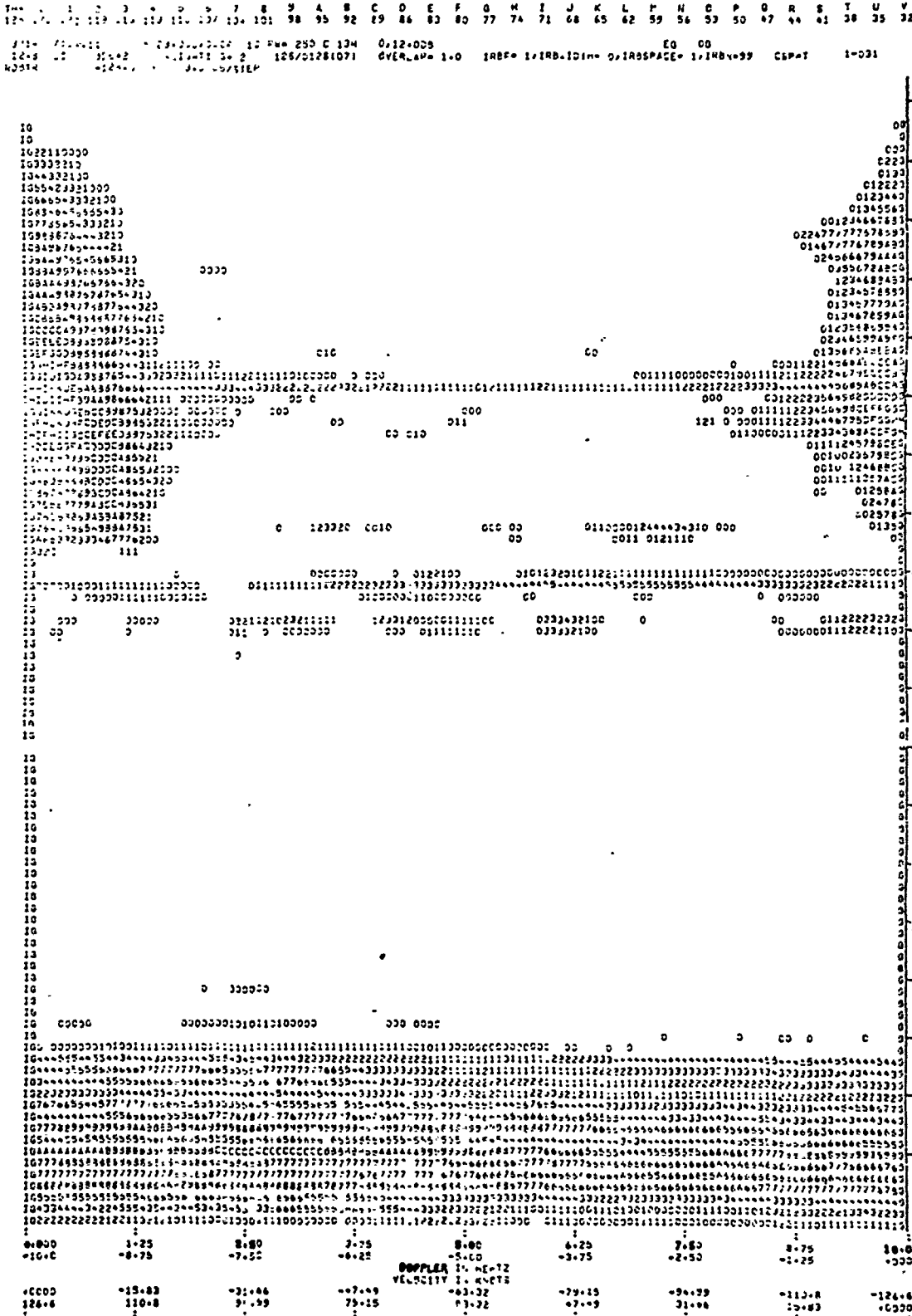
Threshold = 128 dBm
Scale = 3dB per step
Beam 13 Vertical
6.4 minute average

(U) Fig. 5 - Beam 13, Vertical, 10 PRF, 6.4-minute average.

SECRET

Copy available to DDC does not permit fully legible reproduction

SECRET

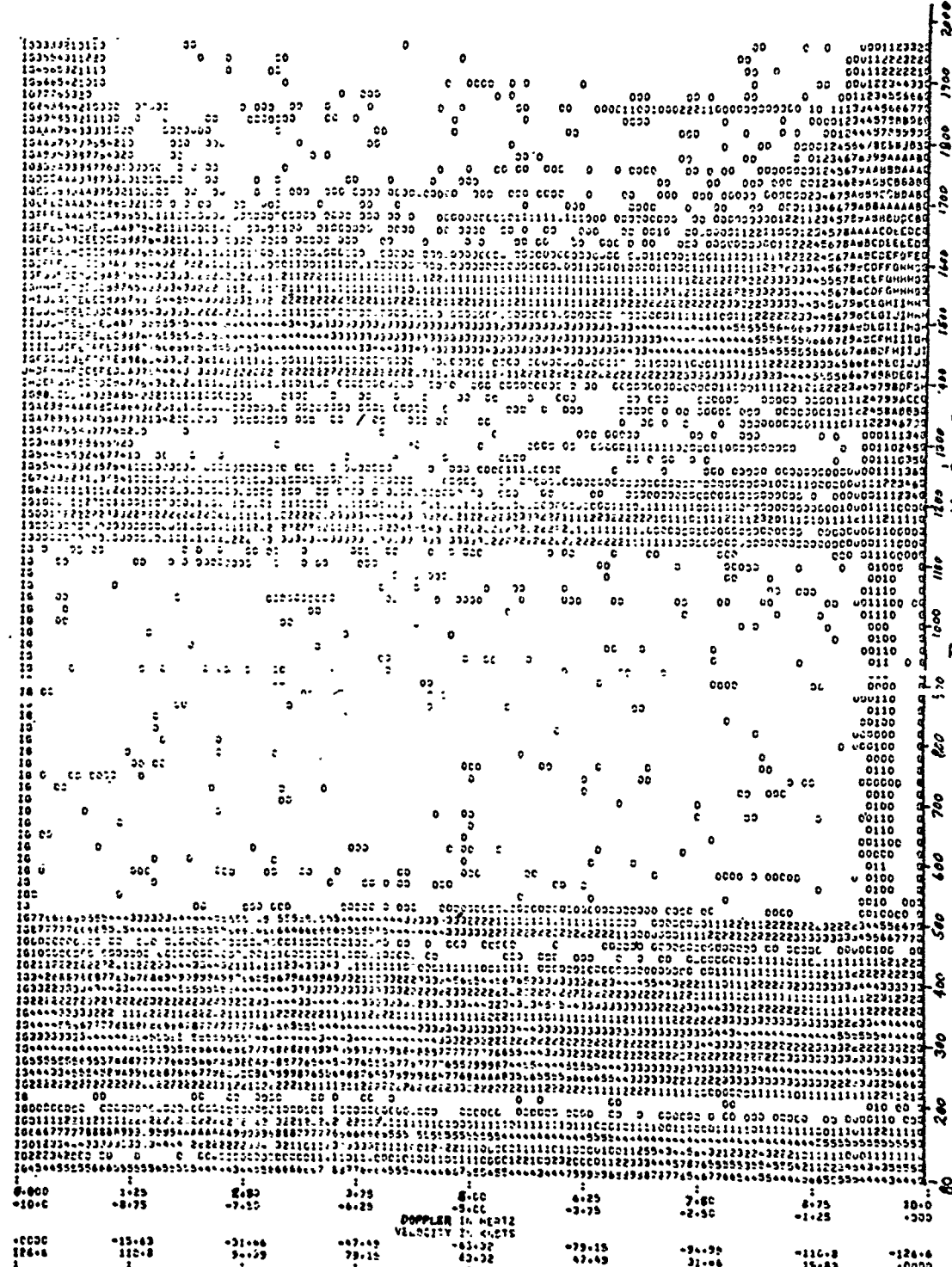


(U) Fig. 6 - Beam 13, Horizontal, 10 PRF, 6.4-minute average.

Copy available to DDC does not permit fully legible reproduction

SECRET

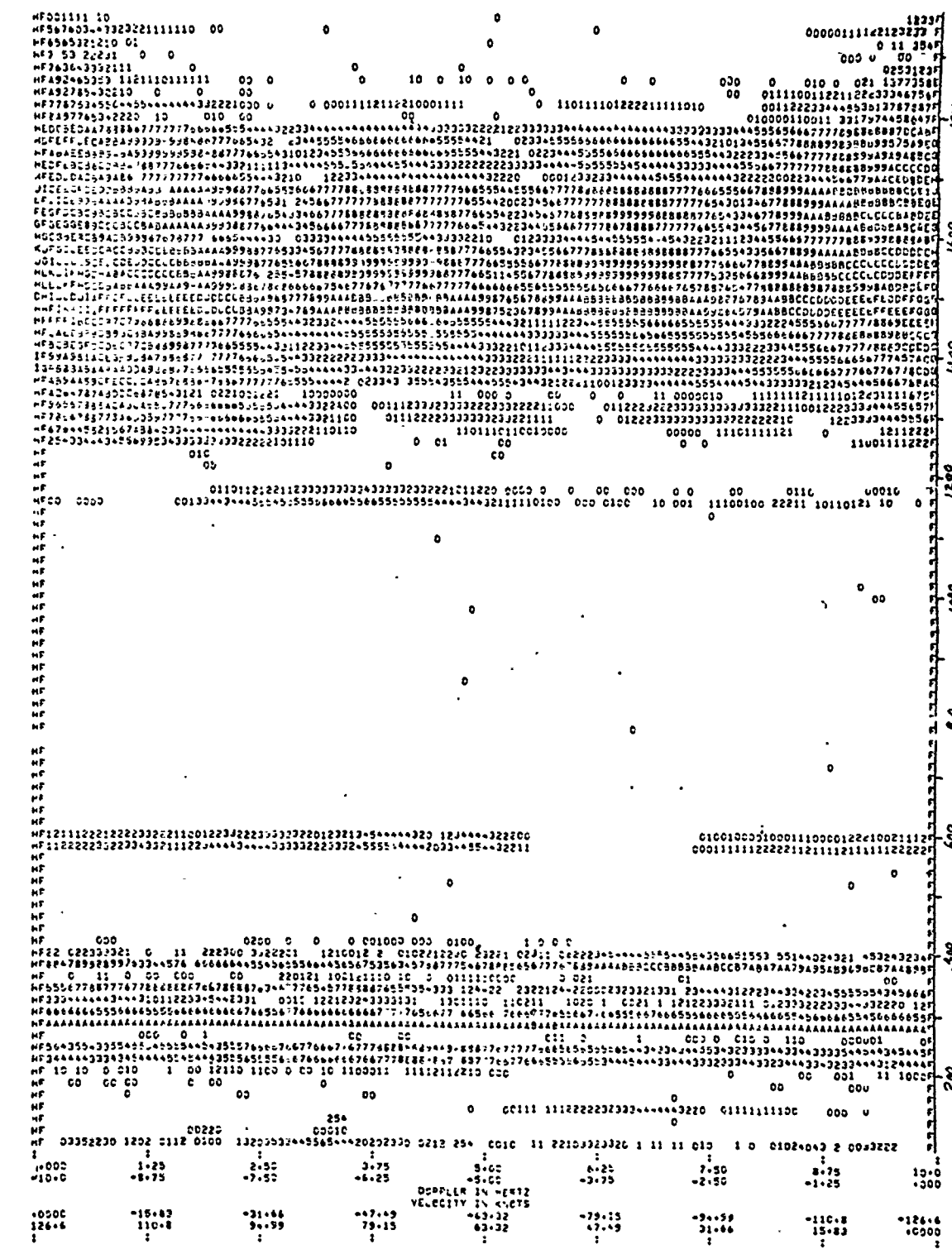
123 124 125 126 127 128 129 130 131 132 133 134 135 136 137 138 139 140 141 142 143 144 145 146 147 148 149 150 151 152 153 154 155 156 157 158 159 160 161 162 163 164 165 166 167 168 169 170 171 172 173 174 175 176 177 178 179 180 181 182 183 184 185 186 187 188 189 190 191 192 193 194 195 196 197 198 199 200 201 202 203 204 205 206 207 208 209 210 211 212 213 214 215 216 217 218 219 220 221 222 223 224 225 226 227 228 229 230 231 232 233 234 235 236 237 238 239 240 241 242 243 244 245 246 247 248 249 250 251 252 253 254 255 256 257 258 259 260 261 262 263 264 265 266 267 268 269 270 271 272 273 274 275 276 277 278 279 280 281 282 283 284 285 286 287 288 289 290 291 292 293 294 295 296 297 298 299 300 301 302 303 304 305 306 307 308 309 310 311 312 313 314 315 316 317 318 319 320 321 322 323 324 325 326 327 328 329 330 331 332 333 334 335 336 337 338 339 340 341 342 343 344 345 346 347 348 349 350 351 352 353 354 355 356 357 358 359 360 361 362 363 364 365 366 367 368 369 370 371 372 373 374 375 376 377 378 379 380 381 382 383 384 385 386 387 388 389 390 391 392 393 394 395 396 397 398 399 400 401 402 403 404 405 406 407 408 409 410 411 412 413 414 415 416 417 418 419 420 421 422 423 424 425 426 427 428 429 430 431 432 433 434 435 436 437 438 439 440 441 442 443 444 445 446 447 448 449 450 451 452 453 454 455 456 457 458 459 460 461 462 463 464 465 466 467 468 469 470 471 472 473 474 475 476 477 478 479 480 481 482 483 484 485 486 487 488 489 490 491 492 493 494 495 496 497 498 499 500 501 502 503 504 505 506 507 508 509 510 511 512 513 514 515 516 517 518 519 520 521 522 523 524 525 526 527 528 529 530 531 532 533 534 535 536 537 538 539 540 541 542 543 544 545 546 547 548 549 550 551 552 553 554 555 556 557 558 559 560 561 562 563 564 565 566 567 568 569 570 571 572 573 574 575 576 577 578 579 580 581 582 583 584 585 586 587 588 589 590 591 592 593 594 595 596 597 598 599 600 601 602 603 604 605 606 607 608 609 610 611 612 613 614 615 616 617 618 619 620 621 622 623 624 625 626 627 628 629 630 631 632 633 634 635 636 637 638 639 640 641 642 643 644 645 646 647 648 649 650 651 652 653 654 655 656 657 658 659 660 661 662 663 664 665 666 667 668 669 670 671 672 673 674 675 676 677 678 679 680 681 682 683 684 685 686 687 688 689 690 691 692 693 694 695 696 697 698 699 700 701 702 703 704 705 706 707 708 709 710 711 712 713 714 715 716 717 718 719 720 721 722 723 724 725 726 727 728 729 730 731 732 733 734 735 736 737 738 739 740 741 742 743 744 745 746 747 748 749 750 751 752 753 754 755 756 757 758 759 760 761 762 763 764 765 766 767 768 769 770 771 772 773 774 775 776 777 778 779 780 781 782 783 784 785 786 787 788 789 790 791 792 793 794 795 796 797 798 799 800 801 802 803 804 805 806 807 808 809 810 811 812 813 814 815 816 817 818 819 820 821 822 823 824 825 826 827 828 829 830 831 832 833 834 835 836 837 838 839 840 841 842 843 844 845 846 847 848 849 850 851 852 853 854 855 856 857 858 859 860 861 862 863 864 865 866 867 868 869 870 871 872 873 874 875 876 877 878 879 880 881 882 883 884 885 886 887 888 889 890 891 892 893 894 895 896 897 898 899 900 901 902 903 904 905 906 907 908 909 910 911 912 913 914 915 916 917 918 919 920 921 922 923 924 925 926 927 928 929 930 931 932 933 934 935 936 937 938 939 940 941 942 943 944 945 946 947 948 949 950 951 952 953 954 955 956 957 958 959 960 961 962 963 964 965 966 967 968 969 970 971 972 973 974 975 976 977 978 979 980 981 982 983 984 985 986 987 988 989 990 991 992 993 994 995 996 997 998 999 1000



Threshold = -128 dBm
Scale = 3 dB per step
Yagi - 6.4 minute average

(U) Fig. 7 - Yagi, 10 PRF, 6.4-minute average

SECRET



Threshold = -125 dBm
Scale = 3 dB per step
(U) Fig. 8 - Beam 13V, 10 PRF, single integration time containing multiplicative noise.

THR 0 1 2 3 4 5 6 7 8 9 A B C D E F G H I J K L M N O P Q R S T U V
 125 122 119 116 113 110 107 104 101 98 95 92 89 86 83 80 77 74 71 68 65 62 59 56 53 50 47 44 41 38 35 32 29

3/14 06:59:12 n 29-000/00CF 10 PW= 250 C 13V 0.12-0DB EO 00
 12.8 SEC MDE#2 EIGHTHIN#7 128/01281071 OVERLAP= 1.0 I&F# 1:1R6W1D7# 0:1R8SPACE# 1:1R8#-39 CSP=T 2-011
 RCD# #125.0 DB# 3.0 DB/STEP

SECRET

Copy available to DDC does not permit fully legible reproduction

SECRET



Range - nautical miles
 2.1 minute average
 10 PRF, 2-minute average not including multiplicative noise burst.

Threshold = -128 dBm
 Scale = 3 dB per step
 (U) Fig. 9 - Beam 13V, 10 PRF, 2-minute average not including multiplicative noise burst.

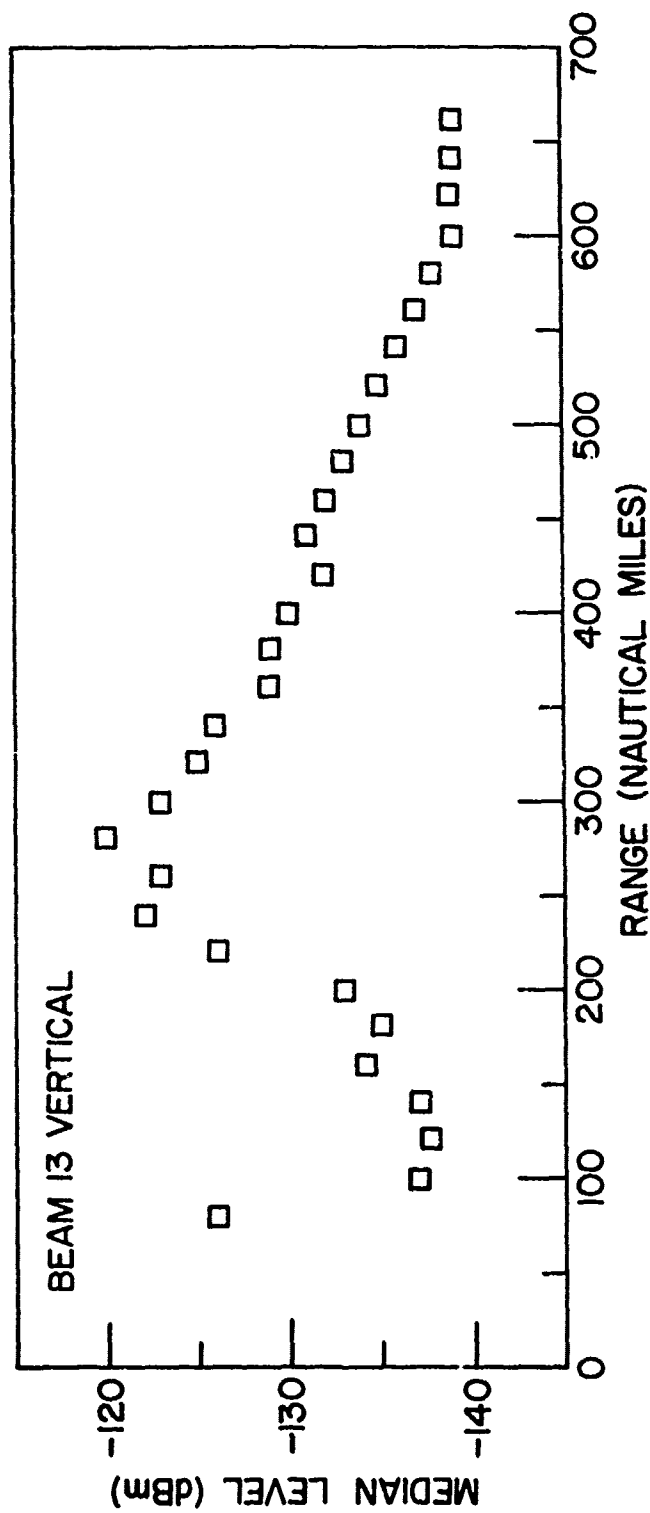
0000	-15.83	-31.66	-47.49	-63.32	-79.15	-94.99	-110.8	-126.6
126.6	110.8	94.99	79.15	63.32	47.49	31.66	15.83	0.00

DOPLER IN HERTZ
 VELOCITY IN KNOTS

THR 0 1 2 3 4 5 6 7 8 9 A B C D E F G H I J K L M N O P Q R S T U V
 125 122 119 116 113 110 107 104 101 98 95 92 89 86 83 80 77 74 71 68 65 62 59 56 53 50 47 44 41 38 35 32 29

3/1 C6156758 M 23.04C0C0F 10 PW= 250 C 13V 0.12-00B EQ CO
 14.8 SEC MODE=2 ALIGHTING= 2 128/01261071 OVERLAP= 1.0 IRSP= 1.18RWIDTH= 0.11RSPACE= 1.18RMS= 5 CSP=1 2.011
 NDC1R =125.0 DBM 3.0 DB/STEP

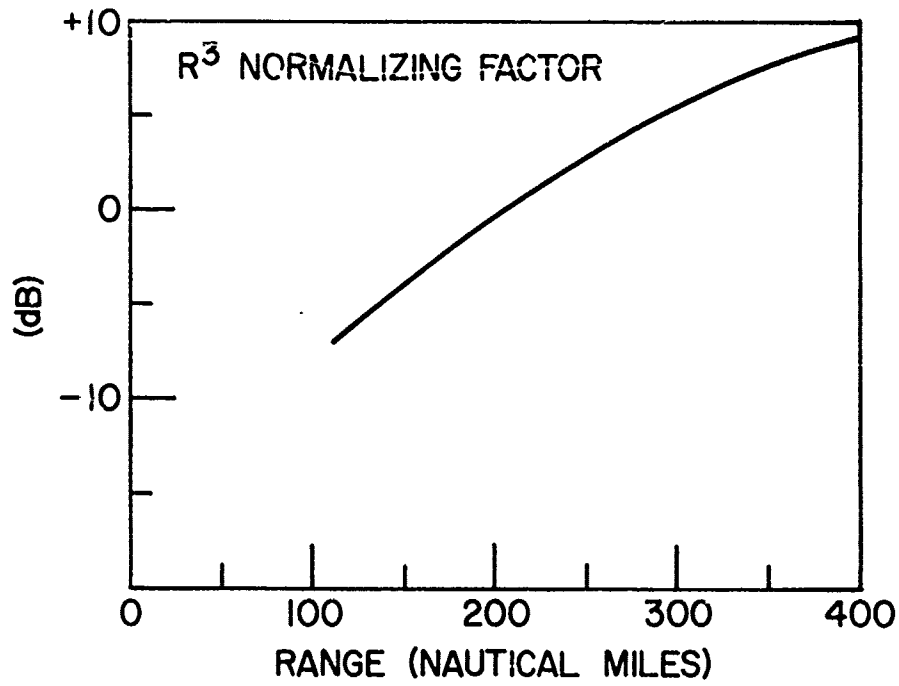
SECRET



(C) Fig. 10 - Beam 13, Vertical - median noise versus range.

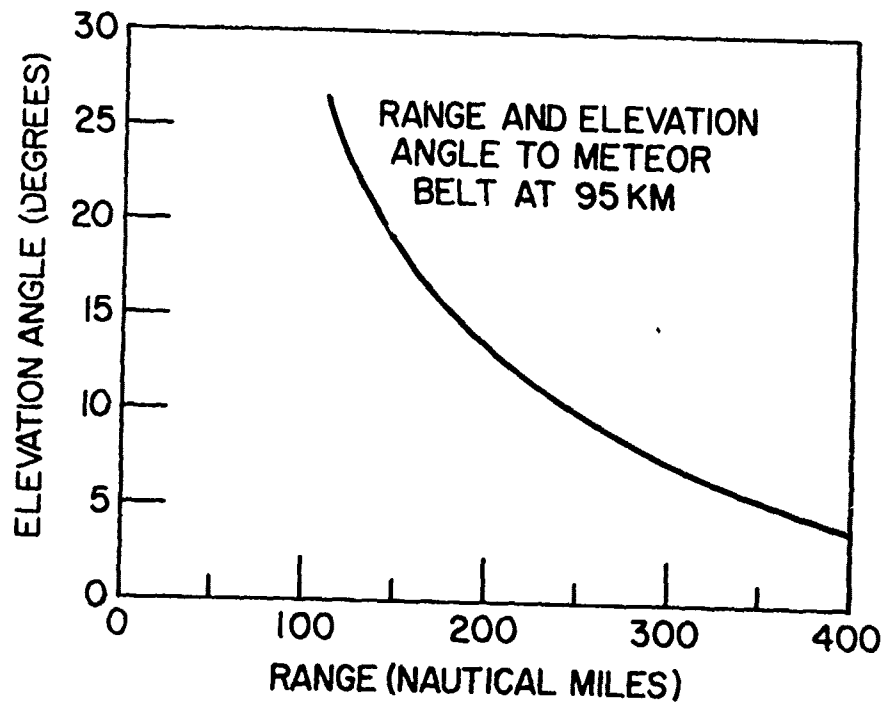
SECRET

SECRET



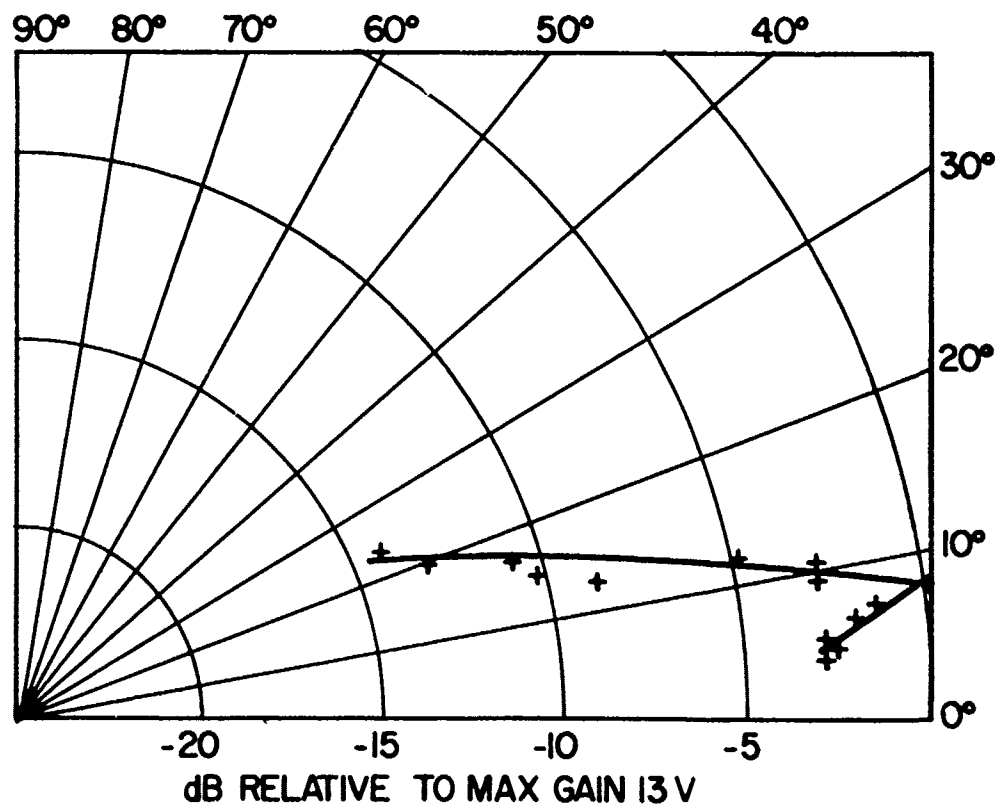
(U) Fig. 11 - R³ normalizing factor used.

SECRET



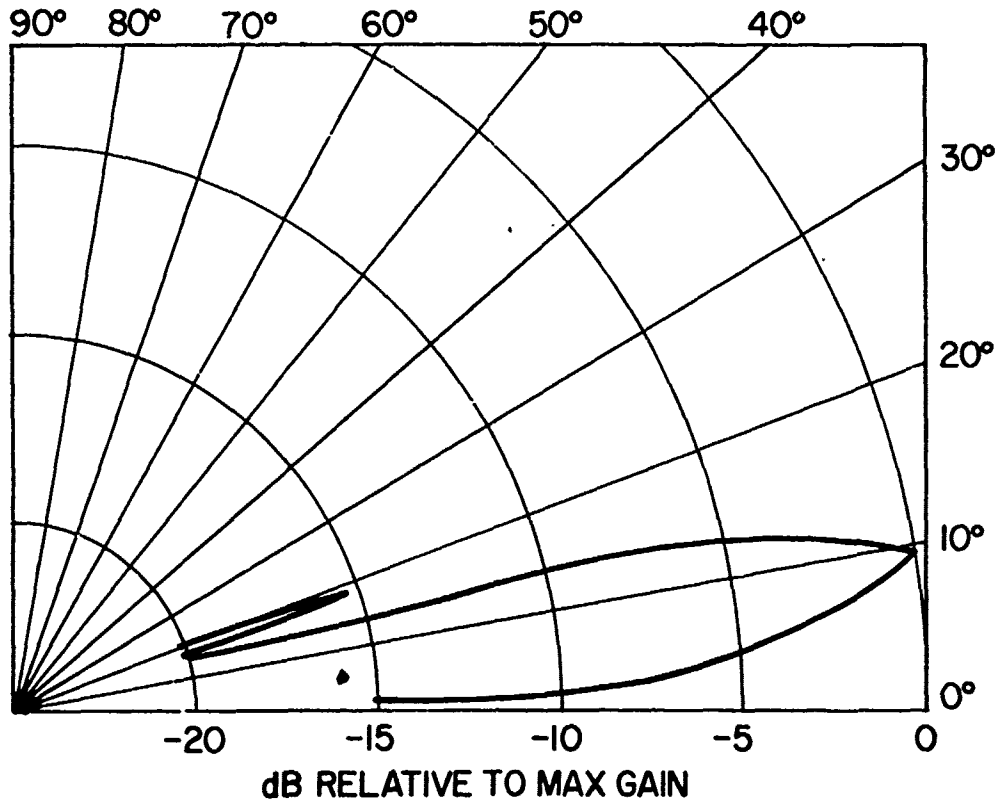
(U) Fig. 12 - Range and elevation angle to meteor belt.

SECRET



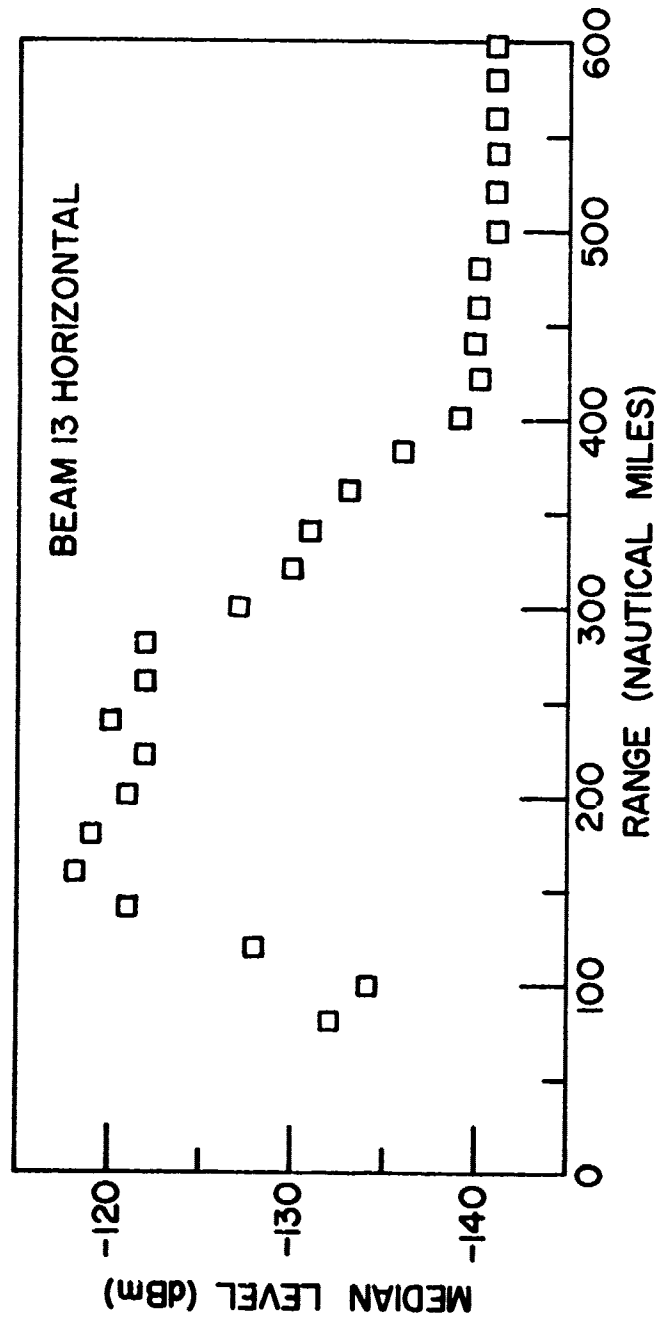
(C) Fig. 13 - Beam 13, Vertical - elevation pattern calculated from meteor data.

SECRET



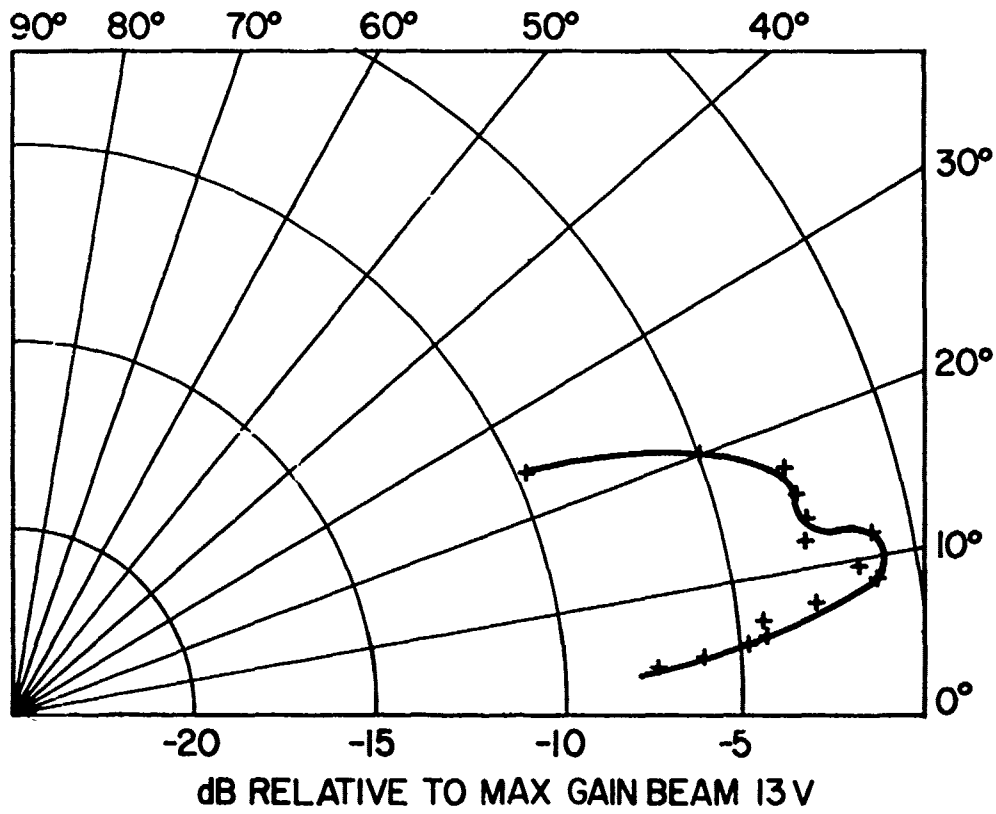
(C) Fig. 14 - Beam 12, Vertical - measured elevation pattern.

SECRET



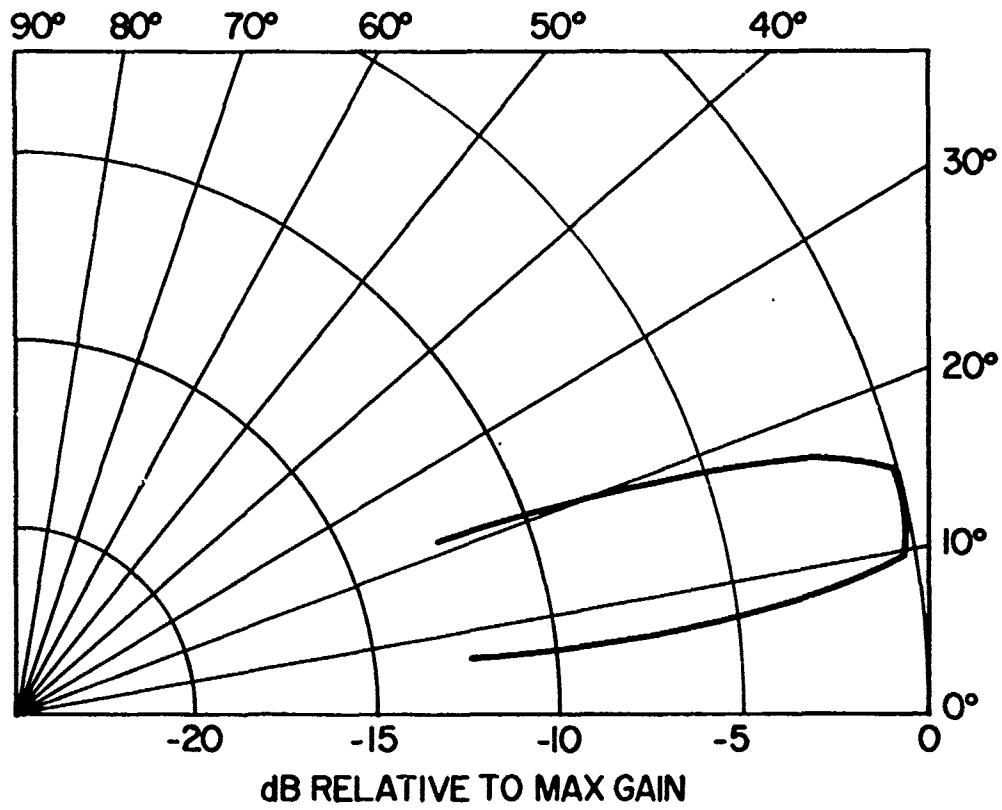
(C) Fig. 15 - Beam 13, Horizontal - median noise versus range.

SECRET



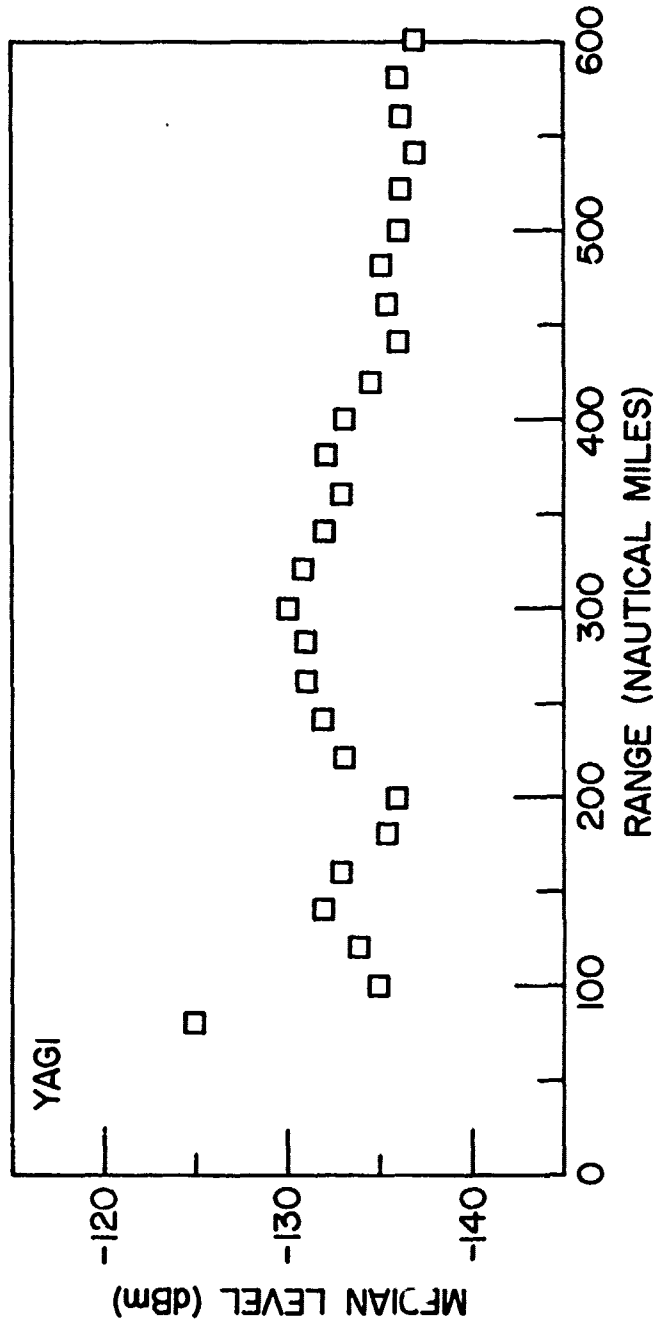
(C) Fig. 16 - Beam 13, Horizontal - elevation pattern calculated from meteor data.

SECRET



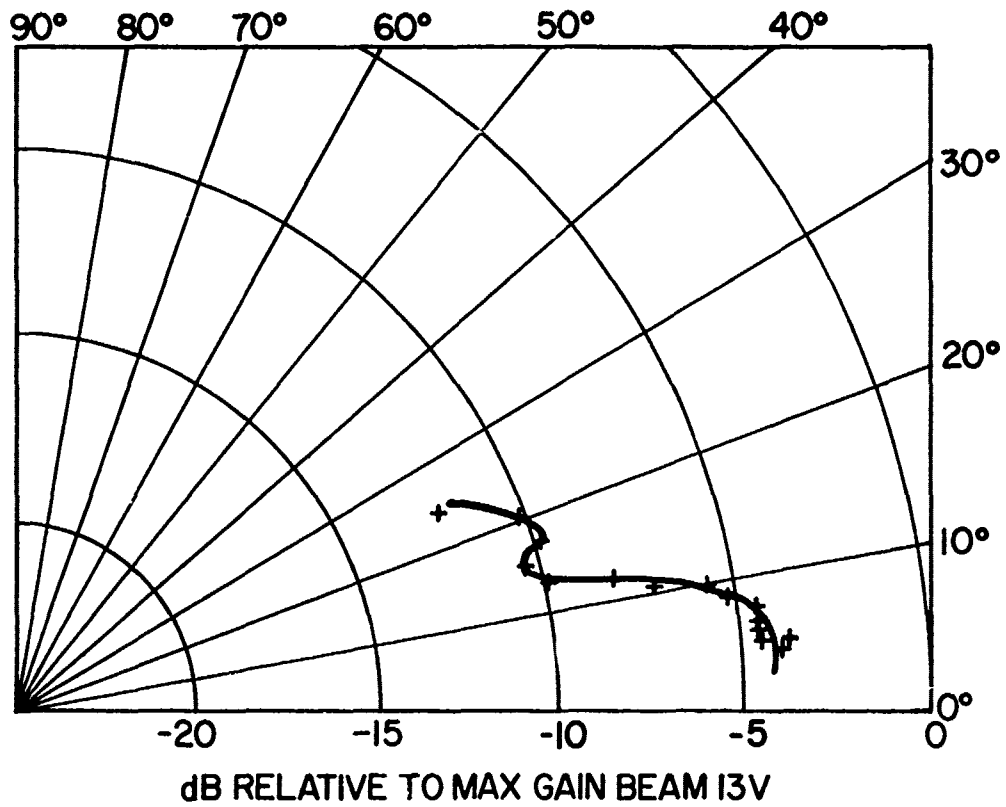
(C) Fig. 17 - Beam 7, Horizontal - measured elevation pattern.

SECRET



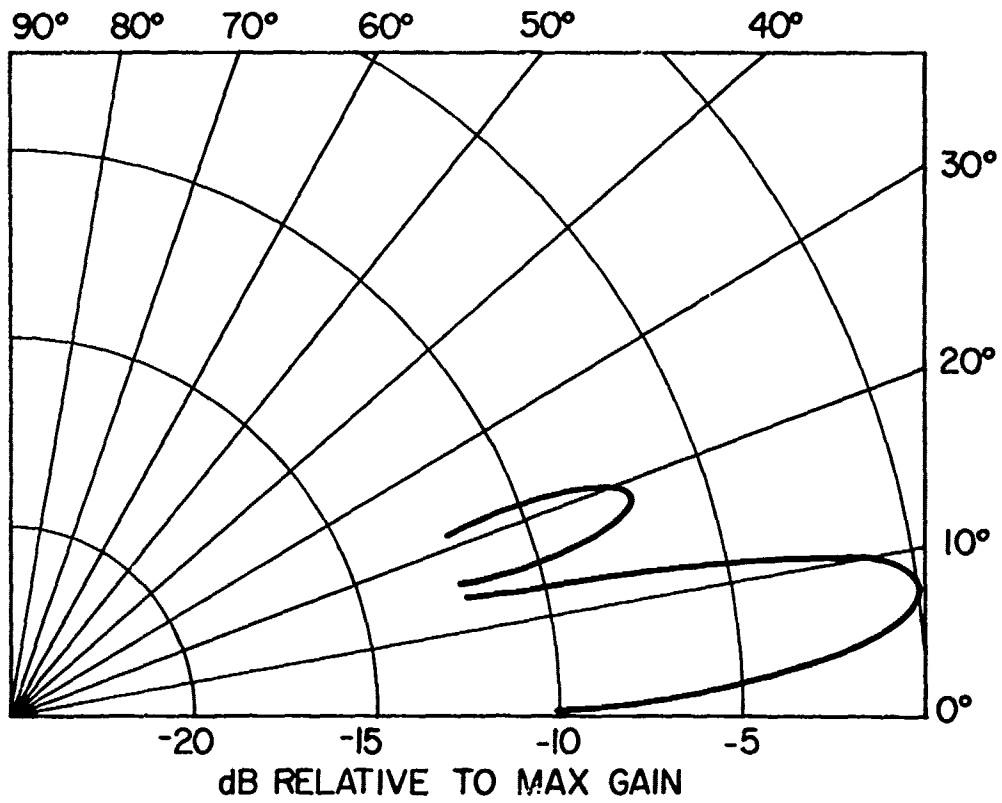
(C) Fig. 18 - Yagi median noise versus range.

SECRET



(U) Fig. 19 - Yagi elevation pattern calculated from meteor data.

SECRET



(U) Fig. 20 - Yagi elevation pattern courtesy of R. Rafuse.

MEMORANDUM

20 February 1997

Subj: Document Declassification

Ref: (1) Code 5309 Memorandum of 29 Jan. 1997
(2) Distribution Statements for Technical Publications
NRL/PU/5230-95-293

Encl: (a) Code 5309 Memorandum of 29 Jan. 1997
(b) List of old Code 5320 Reports
(c) List of old Code 5320 Memorandum Reports

1. In Enclosure (a) it was recommended that the following reports be declassified, four reports have been added to the original list:

Formal: 5589, 5811, 5824, 5825, 5849, 5862, 5875, 5881, 5903, 5962, 6015, 6079, 6148, 6198, 6272, 6371, 6476, 6479, 6485, 6507, 6508, 6568, 6590, 6611, 6731, 6866, 7044, 7051, 7059, 7350, 7428, 7500, 7638, 7655. Add 7684, 7692.

Memo: 1251, 1287, 1316, 1422, [redacted], 1500, 1527, 1537, 1540, 1567, 1637, 1647, 1727, 1758, 1787, 1789, 1790, 1811, 1817, 1823, 1885, 1939, 1981, 2135, 2624, 2701, 2645, 2721, 2722, 2723, 2766. Add 2265, 2715.

The recommended distribution statement for the these reports is: **Approved for public release; distribution is unlimited.**

2. The above reports are included in the listings of enclosures (b) and (c) and were selected because of familiarity with the contents. The rest of these documents very likely should receive the same treatment.

J. M. Headrick
J. M. Headrick
Code 5309

Copy: Code 1221 — *CR OK 7/2/97*
Code 5300
Code 5320
Code 5324